Environ. Water Eng., 2025, 11(4), 461-472 https://doi.org/10.22034/ewe.2025.530499.2035

EWE

Environment and Water Engineering

Homepage: www.jewe.ir

ISSN: 2476-3683

Investigating the effects of land use change on the hydrological behavior of the urban basin

Salar Muhammed Ali[1], Mohsen Isari[1]✉, Haveen Muhammed Rashid[2], Seyed Dana Parizadi[1], and Jamil Bahrami[1]

[1]Department of Civil Engineering, Faculty of Engineering, University of Kurdistan, Sanandaj, Kurdistan, Iran
[2]Water Resources Department, Faculty of Engineering, University of Sulaimani, Sulaymaniyah, Iraq

ARTICLE INFO

Paper Type: Research Paper

Received: 15 June 2025
Revised: 02 August 2025
Accepted: 08 August 2025
Published: 08 August 2025

Keywords
HEC-HMS
Hydrological Modeling
Impervious Surfaces
Land Use
Peak Discharge

Corresponding author:
M. Isari
✉ m.isari@uok.ac.ir

ABSTRACT

Rainfall-runoff modelling is one of the most complex tasks in hydrological studies because it requires accounting for the diverse characteristics of watersheds. This modelling is essential for predicting runoff at watershed outlets by replicating the basin's hydrological dynamics. This study employed the Hydrologic Engineering Centre - Hydrologic Modelling System (HEC-HMS) model to simulate runoff in the Kalar urban watershed, situated in Sulaymaniyah Governorate, Kurdistan Region of Iraq KRI, over the period from 2017 to 2023. Input parameters for the HEC-HMS model were extracted using tools like HEC-GeoHMS and ArcGIS. Various methods were applied throughout the modelling process, including the SCS-CN method for precipitation loss estimation, the SCS-UH method for excess rainfall transformation, and the Muskingum method for flood routing. Furthermore, rainfall-runoff efficiency improved from an average of 70% in 2017–2018 to higher levels in 2022–2023, particularly in basins with reduced losses, such as W270 (87.25%), W260 (87.04%), and W240 (which increased from 83.68% to 89.77%). In addition, the study underscores the significant impact of impervious surface expansion on runoff and peak discharge. The peak discharge at the outlet rose by 6.89%, with moderate increases observed in sub-basins W240 (4.44%) and W260 (5.88%).

Highlights

- The HEC-HMS model accurately simulated rainfall-runoff in the Kalar urban basin.
- Urbanization increased impervious surfaces, leading to higher runoff efficiency and peak discharge.
- Runoff efficiency improved over time due to land use changes.

Citing:
Muhammed Ali, S., Isari, M., Muhammed Rashid, H., Parizadi, S. D., & Bahrami, J. (2025). Investigating the effects of land use change on the hydrological behavior of the urban basin. *Environment and Water Engineering*, *11*(4), 461-472. https://doi.org/10.22034/ewe.2025.530499.2035

1. Introduction

Water is in short supply, and both current usage patterns and potential climate change are anticipated to cause widespread shortages by the mid-21st century. According to the FAO, the need for water is increasing twice as fast as the world's population (Aziz et al., 2023). One solution is to compute runoff using a comprehensive model that includes evapotranspiration, infiltration, and percolation (Patil et al., 2019). Surface runoff estimation supports flood forecasting, groundwater recharge, hydropower generation, and water resource management. Runoff is affected by rainfall characteristics as well as parameters like soil texture, vegetation, slope, and antecedent moisture (Rashid, 2022). Hydrological models are categorized into deterministic and stochastic, as well as lumped, semi-distributed, and distributed models. HEC-HMS is one of the most well-known tools for simulating rainfall-runoff processes (Nchumbeni 2020, and Amini, & Hesami, 2017). The NRCS (SCS) model is widely used to estimate runoff in ungauged basins, especially for water resource planning in arid and semi-arid regions (Ningaraju & SB 2016, and Pal & Samanta, 2011). Increased urbanization will likely lead to more frequent flooding due to higher runoff and shorter response times. Land use/land cover (LULC) changes impact watershed hydrology by increasing impervious surfaces, leading to greater runoff and altered

hydrologic processes (Khzr et al., 2022 and Hu & Shrestha, 2020).

Remote sensing (RS) and GIS have become essential tools in hydrological modeling, enabling accurate spatial and temporal analyses of LULC changes and urban growth (Aswal et al., 2018). In this section, a review of studies conducted using the HEC-HMS model in different regions of the world is presented. In the Gilgel Abay watershed in Ethiopia, which is part of the Lake Tana basin, the HEC-HMS model was implemented using a 30 m resolution DEM and the SCS-CN method, SCS unit hydrograph, and Muskingum method. The results showed that the Curve Number parameter is the most sensitive factor in the model. Statistical criteria indicated high accuracy and a good match between the model and observational data (Tassew et al., 2019). In the United States, in the Richland Creek Watershed, the impacts of land use/land cover (LULC) changes during the 2001 to 2011 period were examined using the HEC-HMS model and Arc Hydro and HEC-GeoHMS tools. The results showed that an 11.21% increase in impervious surfaces led to a 125% to 175% increase in peak discharge (Hu & Shrestha, 2020). In the Erbil basin in the Kurdistan Region of Iraq, land use changes from 1984 to 2019 were studied. HEC-GeoHMS and HEC-HMS models were used to analyze the effects of these changes on urban flooding. The results indicated that over these 35 years, the peak discharge increased from 392.2 m^3/s to 450 m^3/s and the runoff volume increased from 27.4 mm to 30.9 mm (Mustafa & Szydłowski, 2020a). In the Diyala River basin, conceptual and distributed models of HEC-HMS and GeoHMS with spatial data and DEM were used for the 2017 to 2021 period. CN values ranged between 60 to 100, and the difference between measured and simulated peak discharge at the Hemrin Dam station was very small, ranging from +0.1 to −0.2% (Alrammahi & Hamdan, 2022). In the Khabur River basin, the impact of climate change on runoff was analyzed using the HEC-HMS model and CFSR reanalysis data. Daily streamflow at the Zakho station was simulated, and the model was calibrated, resulting in a good match with observed data. Various RCP scenarios were also analyzed to predict the future during the 2021–2030, 2041–2050, and 2061–2070 periods (Haitham & Al-Mukhtar, 2022). To evaluate runoff volume and flood hazard in the Al-Azim River basin in Iraq, the HEC-HMS model was used with daily rainfall data for the 2015 to 2018 period. Despite a good match between simulated and observed discharge, the total volume of simulated discharge was overestimated (Hamdan et al., 2021). In the Al-Kawser basin, located in the northeast of Nineveh province, surface runoff from 1986 to 2018 was modeled using the Snyder method and the HEC-HMS model. The results showed that the annual runoff volume varied between 1361 to 19706 thousand cubic meters, and installing rainwater harvesting systems was recommended to combat water scarcity (Maher et al., 2022). In the Kanarouh River basin (a sub-basin of the Lesser Zab River), five different models, including HEC-HMS, Snyder, TR55, HEC-1, and the Rational method, were compared for estimating peak discharge and time to peak. The Snyder and TR55 models showed better agreement with field data, while HEC-HMS yielded the highest peak discharge (800 m^3/s) (Mohammed et al., 2023). Finally, in the city of Erbil, flood risk was analyzed using the HEC-RAS 2D hydrodynamic model and topographic, LULC, and soil data. The results indicated that lower elevation areas of the city and regions with high rainfall had the highest vulnerability to flooding (Mustafa et al., 2023b).

A review of the studies shows that the HEC-HMS model, when integrated with GIS tools, HEC-GeoHMS, and parameter sensitivity analysis, has a high capability in accurately simulating hydrological processes. The Curve Number parameter has been introduced as the most sensitive factor in most studies, and validation of the model's using indices such as NSE, R^2, and RMSE indicates high simulation accuracy. Furthermore, the impact of land use changes and climate change on increasing runoff and peak discharge has been clearly confirmed in the results of multiple studies. This research focuses on the Kalar district in Sulaimaniyah Governorate, where recent urban development has significantly changed land use and raised flood risks. Modeling the relationship between LULC change and surface runoff using HEC-HMS is vital for sustainable urban planning and disaster management. Accordingly, the main objective of this study is to simulate rainfall-runoff processes in the Kalar urban watershed using the HEC-HMS model, assess the hydrological impacts of recent LULC changes, and provide sub-basin-specific recommendations to support flood risk mitigation and water resource planning.

2. Materials and methods

2.1 Study area

The Kalar city is the administrative center of the Garmian region, located south of the Sulaymaniyah Governorate-Iraq, about 80 km from Sulaymaniyah city (Fig. 1). The study area describes the urban basin in Kalar, which encompasses 438 km^2 and is located between latitudes 34°33'0" N to 35°9'0" N and longitudes 44°54'0" E to 45°35'0" E. The topography of the urban basin chosen in the current study ranges between 190 to 930 m above mean sea level according to the Digital Elevation Model (DEM) acquired from UGS Earth Explorer with a spatial resolution of 30 m.

2.2 Data collection

According to LULC 2023, the total urban area of Kalar City is 39.81 km^2, and information from the Kalar Directory of Meteorology and Seismology indicates the average annual rainfall in the Kalar district during the study period (2017–2023) ranged from approximately 110 mm (in 2021) to nearly 690 mm (in 2019), with a multi-year average of 302.02 mm. The rainy season begins in October and ends in April. For model simulation, daily rainfall data from 2017 to 2023, obtained from the Kalar meteorological station, is used.

2.3 Method

2.3.1 HEC-HMS

Accurate prediction of rainfall and runoff is essential for hydrological analysis and planning. Rainfall-runoff models, such as HEC-HMS, are widely used for simulating river flows under varying conditions (Ross et al., 2018). HEC-HMS simulates runoff through sub-basins, reservoirs, junctions, and other elements, using tools like HEC-GeoHMS (Nchumbeni, 2020, and Diriba, 2023). DEM of the study basin is utilized to ascertain the physical properties of the basin for rainfall-runoff (R-R) modeling. ArcGIS 10.4 software has been used for this purpose. From DEM terrain, the basin and river-stream

network has been delineated. For the identification of the streams and sub-basins, the pre-processing menu was used. In addition, the basin properties, including area, stream length, and slope, are calculated using HEC Geo-HMS (Haddad & Remini, 2021). Following the computation of the streams and sub-basins' physical attributes, several hydrological metrics were examined using HSG and LULC maps. These parameters can be assessed as grid-based values or as averages for the sub-basins. The methods selected for the sub-basins under the 'Select HEC-HMS' were Soil Conservation Service-Curve number (SCS-CN), SCS Unit Hydrograph, and Muskingum methods in which they used for loss, transformation, and routing calculations, respectively. Each method is described individually in the following sections.

Fig. 1 Overview of the study area

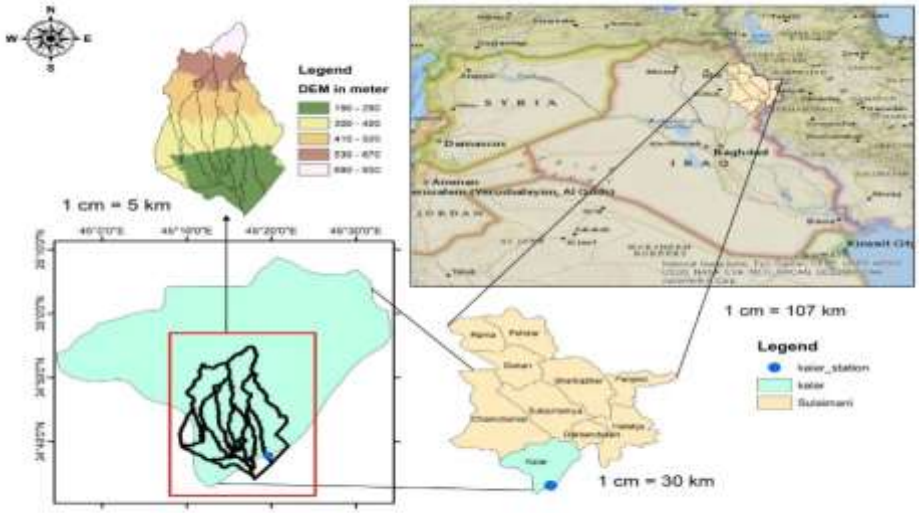

2.3.2 Loss model

The Soil Conservation Service Curve Number (SCS-CN) method was applied to determine the direct runoff from a design rainfall. The initial abstraction (I_a) and the curve number (CN) are two crucial factors in this loss model. The HEC-Geo HMS toolset, which is integrated with ArcMap 10.4, was used to estimate the curve number (CN), which is dependent on DEM, HSG, and LULC maps. The estimating procedure also took into account the proportion of impermeable surfaces (Usda, 1986).

2.3.3 Routing

The effects of channel storage cause flood runoff to decrease as it passes through a channel reach. The Muskingum method, a popular flow routing methodology, is employed in the HEC-HMS model to address this process using Eq. 1. The dimensionless coefficient X, which ranges from 0 to 0.5, indicates how flow affects the channel's storage levels. In addition, the proportionality coefficient K represents the travel time through a river reach (Ibrahim-Bathis and Ahmed, 2016).

$$S = KQ + KX(1 - Q) \quad (1)$$

where KQ is prism storage in the reach, K is the proportionality coefficient, KX (I − Q) is volume of the wedge storage, and X is the weighting factor ($0 \le X \le 0.5$).

2.3.4 Model calibration and validation

A validated model is one whose accuracy and predictive abilities throughout the validation period are within an acceptable range. After optimizing the parameters, the model was evaluated with the calibrated parameters as input throughout the validation period. The validation was carried out for one event in 2023, using the same approach as the calibration process; the obtained results were examined using R (Eq. 2) (Gharibreza et al., 2018; Wang et al. 2016).

$$R = \frac{\left[\sum_{i}^{n}(O_t - O)(S_t - S)\right]}{\sqrt{\sum_{i}^{n}(O_t - O)\sum_{i}^{n}(S_t - S)^2}} \quad (2)$$

where O_t is the observed flow at time, O is the average observed flow at time, S_t is the simulated flow at time, and S is the average simulated flow at the time.

Calibration is an iterative process that involves assessing and fine-tuning model parameters (Ahmadpari and Khaustov, 2025). In order to improve the alignment between simulated and observed data, calibration was carried out in this study to ensure the best possible fit between the observed and simulated data during the calibration period. In addition, the coefficient of determination (R^2) between simulated and observed discharge before and after calibration was presented in Fig. 2. The coefficient of determination (R^2=0.9424) resulting in Fig. 2a, suggests a good fit between observed and simulated discharge data before calibration. However, there is room for improvement, as the scatterplot indicates slight deviations of some points from the trend line. In addition, the coefficient of determination (R^2=0.9575) resulted in Fig. 2b, after the calibration value has improved, indicating a stronger correlation between observed and simulated discharge.

2.3.5 Model performance evaluation

Statistical measures, including correlation coefficient (R), root mean square error (RMSE) (Eq. 3), and Nash-Sutcliffe Efficiency (NSE) (Eq. 4), were used to evaluate the model's performance. The formulas for these evaluations are as follows: The correlation coefficient was calculated by using the following formula (Amini et al., 2009; Wang et al., 2016;).

Fig. 2 Coefficient of determination: a) before calibration and b) after calibration

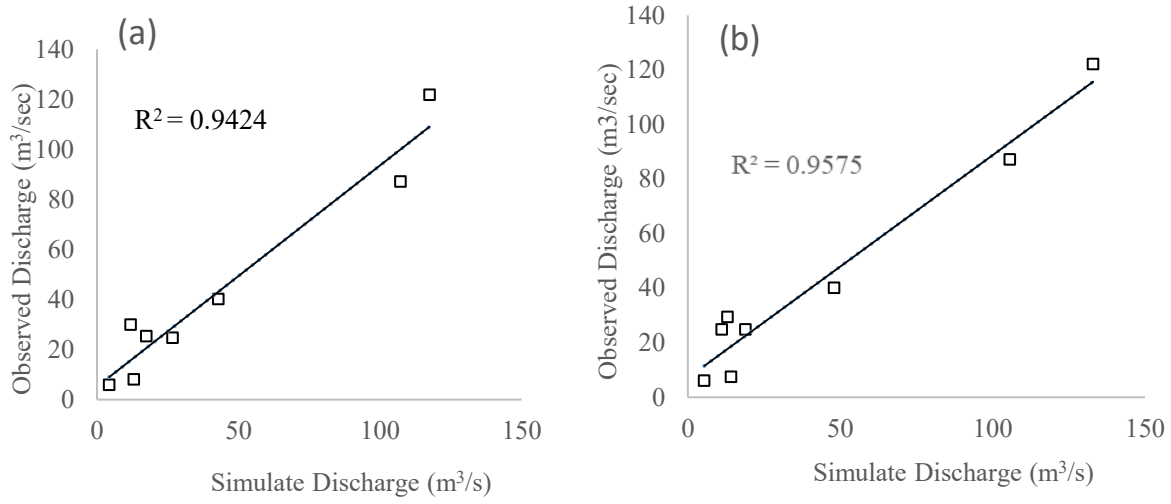

$$RMSE = \sqrt{\frac{1}{n}\sum_{i}^{n}(S_i - O_i)} \quad (3)$$

where: S_i is the simulated flow at time, and O_i is the observed flow at time. The Nash-Sutcliffe Efficiency (NSE) was determined using Eq. 8 (Karami Moghadam et al., 2020).

$$NSE = 1 - \frac{\sum_{i}^{n}\left(Q_{obs,i} - Q_{sim,i}\right)^2}{\sum_{i}^{n}\left(Q_{obs,i} - \overline{Q}_{obs}\right)^2} \quad (4)$$

The meanings of some parameters in Eq. 4 are as follows: Q_{obs} is observed discharge data at the time, Q_{sim} is simulated discharge data at the time. $\overline{Q}_{obs}$ is the mean of observed discharge data, and N is the number of observations. According to Table 1, the model performs admirably, with high NSE values (>0.9), strong correlation coefficients (R) (0.94-0.96), and significantly reduced RMSE after optimization, indicating its ability to accurately simulate runoff and generalize well during both calibration and validation periods. These results show that the model is resilient and trustworthy, allowing you to reliably simulate runoff for subsequent years within the same catchment.

Table 1 Model performance parameters

Metric	Calibration Period		Validation Period
	Before Optimization	After Optimization	
NSE	0.902	0.926	0.923
R	0.94	0.96	0.96
RMSE	0.87	0.63	0.31

3. Results and Discussion

This chapter presents the results of the simulation of rainfall runoff conducted in the urban watershed in Kalar District using the HEC-HMS framework. The analysis focuses on evaluating the model's performance in simulating hydrological responses within the study area. the first section presents the results of the creation CN grid map in HEC-GeoHMS, while in the next section, the results of all sub-basin characteristics were tabulated. Then, the simulation run results for all the individual years from 2017 to 2023 are discussed. Later, the model optimization results, followed by model calibration and model validation, were presented. Finally, the model performance was qualified.

3.1 LULC maps

Sentinel-2 land use/land cover time series of the world are used from 2017 to 2023, as mentioned in chapter three. These maps were extracted for the study area in ArcGIS for the study duration. The extracted LULC was divided into four groups: crops, built-up, barren ground, and range land. Fig. 3 displays the equivalent land use maps for the years 2017, 2018, 2019, 2020, 2021, 2022, and 2023, respectively. The area of each class within the study area, along with the percentage of the class area for each year of the study duration, is presented in Table 2.

The percentage changes in land use patterns across the years presented in Table 3, which highlight dynamic shifts, are discussed below: The crop category shows dramatic fluctuations, with a significant decline of 28.2% from 2017 to 2018, followed by an extraordinary increase of 141.61% in 2019, likely indicating a period of agricultural expansion or recovery after the decline. However, another sharp decrease of 70.69% occurred in 2021, reflecting possible challenges like unfavorable climatic conditions, land conversion, or policy impacts. A substantial recovery of 103.81% in 2023 underscores the volatility in this category. The built-up area demonstrates consistent growth, with small but steady increases every year. The most notable growth occurred from 2018 to 2019 (14.72%) and 2022 to 2023 (9.22%), reflecting continuous urbanization and infrastructure development driven by socio-economic growth and population expansion. The barren ground shows a consistent downward trend, with significant reductions between 2017 and 2019 (-32.81% and -39.57%) and smaller declines in subsequent years. This pattern suggests efforts to rehabilitate or convert barren land into other uses like agriculture or urban areas, or natural vegetation recovery. The Rangeland category exhibits varied trends. It

experienced an increase of 11.22% in 2018 but declined sharply by 25.63% in 2019, likely due to competition with croplands or environmental pressures. A major rebound of 44.40% in 2021 indicates a shift back to range land use, possibly due to changing land management practices or reduced agricultural activities. However, it declined modestly from 2022 to 2023 (-14.84%), showing signs of ongoing competition for land.

Fig. 3 Land use and Land cover of the years 2017-2023

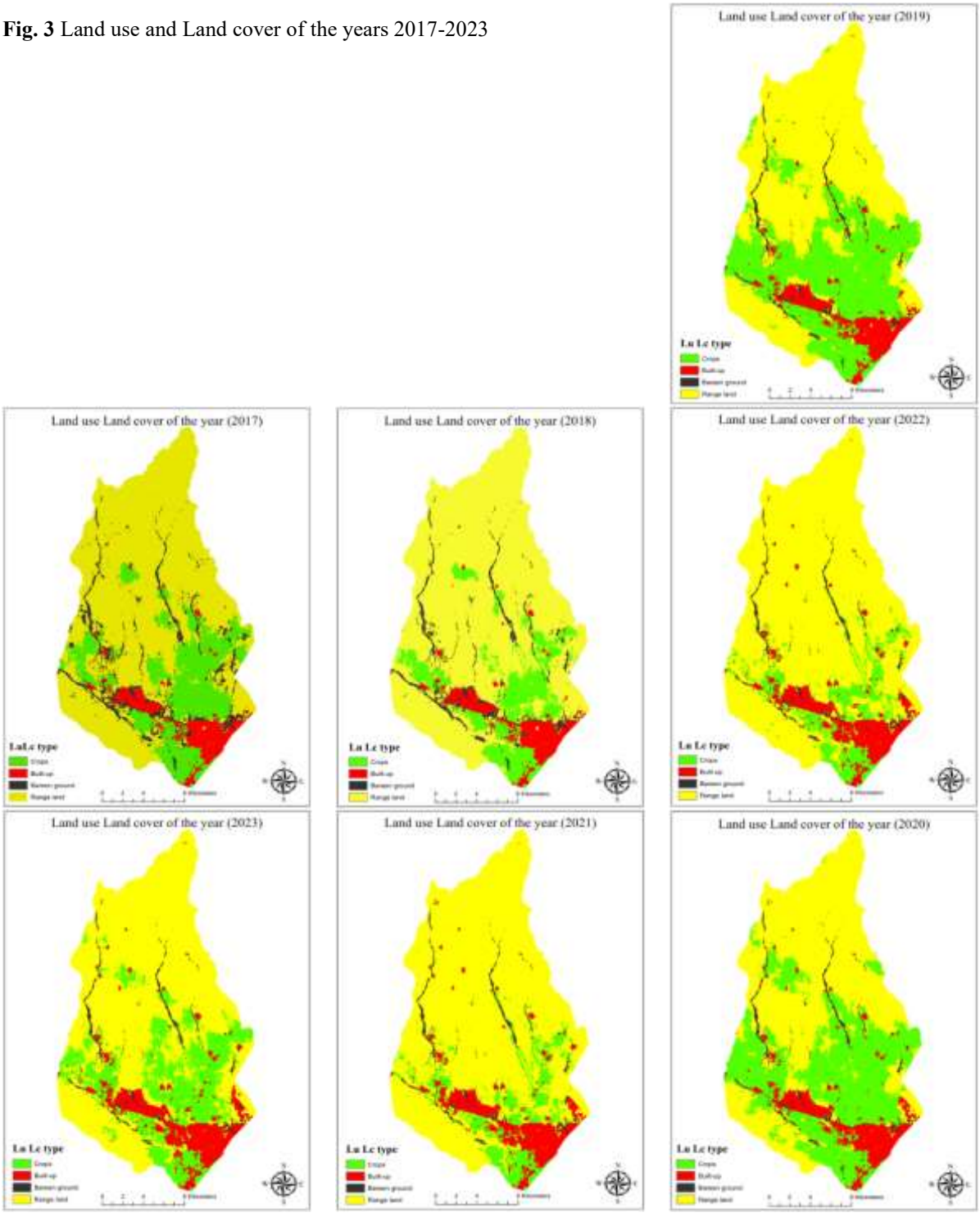

3.2 Curve number

The CN grid map was created by combining the polygons from both the HSG map and the LULC map, as mentioned in the previous chapter. Assigning curve numbers to each sub-basin was the main goal of the CN grid map when the SCS loss approach was chosen because this parameter is necessary for the model to run. The possible maximum soil retention is estimated using the curve number (CN). For impermeable surfaces, its value is 100; for other surfaces, it is $0 < CN \leq 100$. Land use, hydrological soil group, hydrological circumstances, and antecedent moisture condition (AMC) are some of the elements that affect the maximum potential storage linked to the CN. The values of CN vary from 100 for water bodies to around 30 for highly permeable soils with high infiltration capacities (Choudhari et al., 2014). The CN grid

map for the basin was overlaid with the sub-basin boundaries. The zonal statistics tool in ArcGIS was applied to calculate the average Curve Number (CN) for each sub-basin. This ensures an accurate representation of the hydrological characteristics within each sub-basin. Fig. 4 displays the CN number of each sub-basin for the years 2017, 2018, 2019, 2020, 2021, 2022, and 2023, respectively.

Table 2 Overview of various LULC categories

LULC Class	2017		2018		2019		2020		2021		2022		2023	
	Area (km^2)	Area (%)	Area (km^2)	Area (%)	Area (km^2)	Area (%)	Area (km^2)	Area (%)	Area (km^2)	Area (%)	Area (km^2)	Area (%)	Area (km^2)	Area (%)
ops	86.96	19.8	62.44	14.2	150.9	34.4	154.3	35.2	45.21	10.3	46.72	10.7	95.22	21.7
Built-Up	25.87	5.9	26.7	6.09	30.63	6.98	33.37	7.61	36.3	8.27	36.45	8.31	39.81	9.07
Barren Ground	29.26	6.67	19.66	4.48	11.88	2.71	10.69	2.44	10.03	2.29	10.85	2.47	10.14	2.3
Range Land	296.7	67.6	330	75.2	245.4	55.9	240.5	54.8	347.2	79.1	344.7	78.6	293.6	66.9

Table 3 The percent change in area (%) of LULC classes

LULC Category	2017-2018	2018-2019	2019-2020	2020-2021	2021-2022	2022-2023
Crops	-28.2	141.66	2.27	-70.69	3.4	103.94
Built-up	3.22	14.68	9.03	8.67	0.48	9.14
Barren Ground	-32.81	-39.51	-9.96	-6.15	7.86	-6.48
Range Land	11.22	-25.63	-2.02	44.4	-0.72	-14.83

Fig. 4 CN number of each sub-basin for the years 2017-2023

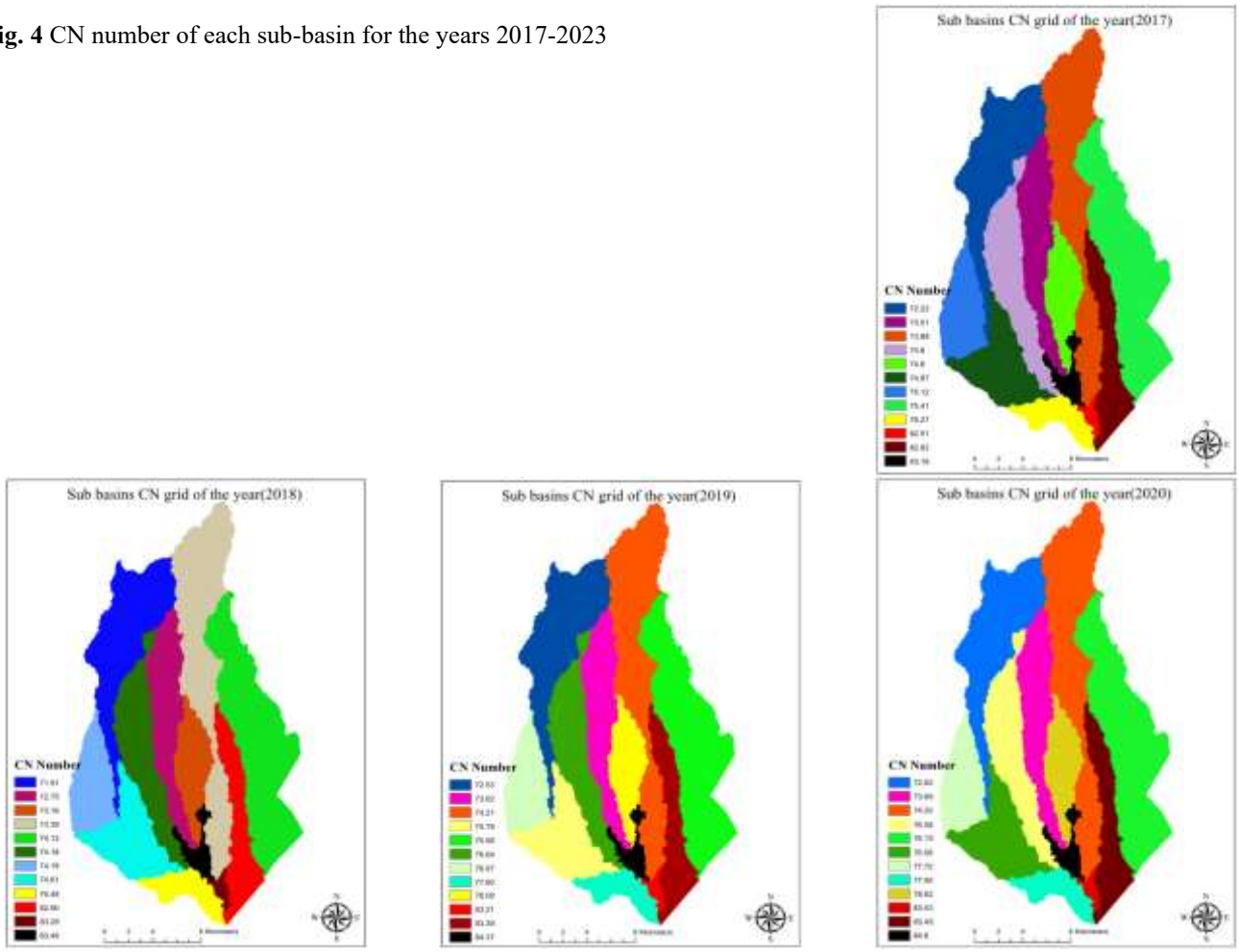

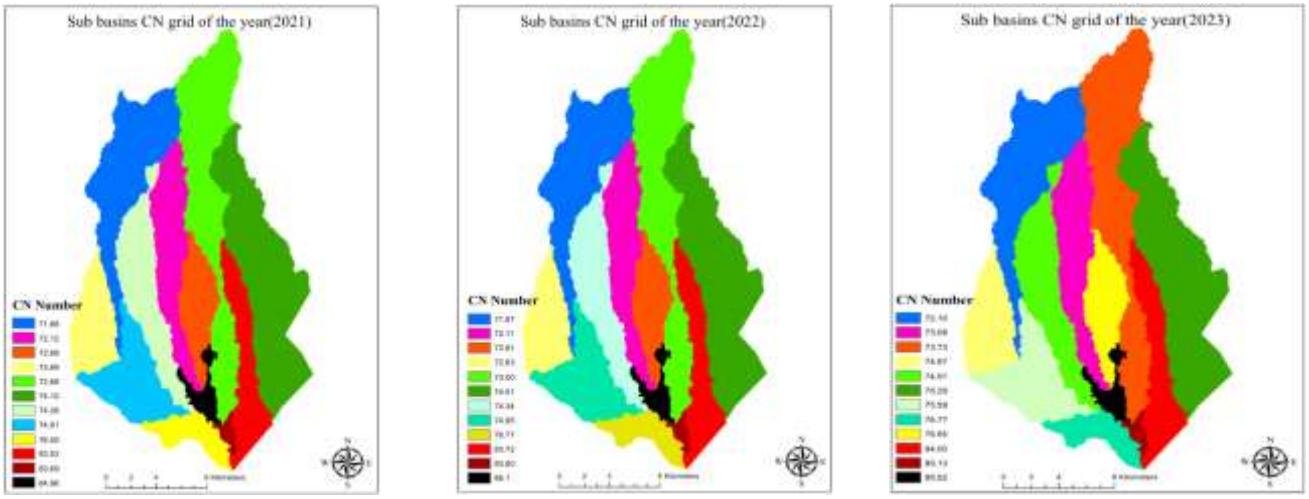

Table 4 Sub-basins Characteristics

Basin Name	Basin Slope %	Longest Flow Pass Meter	Total Area of Basin km^2
W160	4.23	94166	57.30
W170	4.83	133058	77.57
W180	3.51	98213	75.52
W190	3.62	81447	38.60
W200	2.12	39476	27.04
W210	2.44	49079	34.32
W220	2.09	51731	23.88
W230	2.88	87197	41.93
W240	1.59	28767	7.98
W250	2.33	33453	14.92
W260	1.64	17123	3.10
W270	1.72	85122	36.60

The details of the constant characteristics of each 12 individual sub-basins in the study area, including Basin slope (%), longest flow pass, and the total area of the basin in square km, are presented in Table 4.

3.3 Parameter sensitivity analysis

To determine which factors have the biggest effects on model outputs, sensitivity analysis is carried out. The goal of this procedure is to modify parameters in a way that boosts the model's effectiveness or performance. The sensitivity analysis in this study was carried out following the execution of the HEC-HMS model. Variations in some parameters were found by the analysis, which showed that the Curve Number and Lag Time were the most important parameters. Muskingum X and K values increased in the optimization results; however, SCS Curve Number and Lag Time values decreased. Similar results were obtained from the rainfall-runoff simulation using HEC-HMS, with Initial Abstraction, Curve Number, and Lag Time being shown to be the most important parameters (Hamdan et al., 2021; Choudhari et al., 2014). The details of the initial and optimized parameter values are presented in Table 5.

Table 5 Details of parameter optimization

Element	Parameter	Unit	Initial value	Optimize value
R120	Muskingum – K	hr	2.5	10
R70	Muskingum – K	hr	2.5	12
R50	Muskingum – x	-	0.3	0.1
R50	Muskingum – x	-	0.3	0.1
W220	SCS Curve Number - Curve Number	-	78.8	70
W230	SCS Unit Hydrograph - Lag Time	min	443.78	400
W200	SCS Curve Number - Initial Abstraction	mm	15.2	10
W250	SCS Unit Hydrograph - Lag Time	min	230.35	201
W190	SCS Curve Number - Curve Number	-	73.82	67.2
W260	SCS Curve Number - Initial Abstraction	mm	10.19	7

3.4 HEC-HMS Simulation Runs

The hydrologic modeling process involved conducting seven separate HEC-HMS simulations to analyze the basin's hydrological response for the years 2017–2018 through 2022–2023.

3.4.1 Simulation Run for the Water Year 2017- 2018

The simulation run for the year 2017–2018 provides data on precipitation, runoff, loss, rainfall-runoff efficiency, and peak discharge across various sub-basins (W160 to W270) and the outlet. A detailed description of the model run is shown in Table 6. Each basin received the same amount of precipitation,

260.46 mm; however, the runoff, loss, and other parameters varied significantly among the basins, reflecting differences in hydrological behavior and catchment characteristics. The runoff values ranged from 171.34 mm in W160 to 224.1 mm in W270, while the corresponding losses ranged from 36.36 mm in W270 to 89.12 mm in W160. The rainfall-runoff efficiency, represented as a percentage, ranged from 65.78% in W160 to 86.04% in W270. Basins with higher efficiencies, such as W270 (86.04%) and W240 (83.68%), demonstrate a strong ability to convert rainfall into runoff, which could be attributed to reduced infiltration or higher impervious surface coverage. In contrast, lower efficiencies, such as W160 (65.78%), indicate higher losses or less efficient runoff generation mechanisms. Peak discharge values varied widely across the basins, from 1.7 m³/s in W260 to 36.3 m³/s in W180. These differences highlight the variability in flow concentration and peak flow behavior among the basins. Notably, W270 and W240, despite having high rainfall-runoff efficiencies, recorded relatively low peak discharges (20.8 m³/s and 4.5 m³/s, respectively), possibly due to storage or delayed flow routing. Conversely, W180 and W170 showed high peak discharge values (36.3 m³/s and 36.1 m³/s, respectively), indicating a rapid response to rainfall. At the outlet, the cumulative runoff was 188.64 mm, with a total loss of 71.82 mm and a rainfall-runoff efficiency of 72.43%. The peak discharge at the outlet was significantly higher than that of individual basins, reaching 178.5 m³/s, which reflects the combined effect of contributions from upstream basins and flow concentration. This high value emphasizes the potential for flooding and necessitates careful management of peak flows at the outlet.

Table 6 The result of a Simulation Run for the Year 2017-2018

Basin Name	Precipitation (mm)	Runoff (mm)	Loss (mm)	Rainfall/Runoff (%)	Peak Discharge (m^3/sec)
W160	260.46	171.34	89.12	65.78	25.6
W170	260.46	178.09	82.37	68.38	36.1
W180	260.46	184.67	75.79	70.90	36.3
W190	260.46	176.46	84	67.75	17.7
W200	260.46	180.79	79.67	69.41	12.8
W210	260.46	184.36	76.1	70.78	16.5
W220	260.46	179.01	81.45	68.73	11.2
W230	260.46	186.06	74.4	71.44	20.2
W240	260.46	217.95	42.51	83.68	4.5
W250	260.46	187.37	73.09	71.94	7.3
W260	260.46	213.2	47.26	81.86	1.7
W270	260.46	224.1	36.36	86.04	20.8
Outlet	260.46	188.64	71.82	72.43	178.5

3.4.3 Simulation Run for the water year 2022-2023

The simulation for 2022-2023 indicates variation in the hydrological responses of basins W160 to W270 and the outlet under 255.15 mm of uniform precipitation input, as represented in Table 7. Runoff values range from 166.62 mm in W160 to 229.05 mm in W240, and losses range from 26.1 mm in W240 to 88.53 mm in W160. Basins like W240 and W260 have the lowest losses and maximum runoff, indicating efficient water conversion systems. In contrast, W160 and W190 exhibit larger losses, indicating significant infiltration or retention within their hydrological systems. Rainfall-runoff efficiency varies between 65.30% in W160 to 89.77% in W240. Basins W240 and W260 have exceptional efficiencies of 89.77% and 87.04%, showing a higher potential to convert rainfall into runoff. W160 has the lowest efficiency, at 65.30%, indicating higher losses and lesser runoff generation. Peak discharge levels range from 0.8 m³/s (W260) to 16.9 m³/s (W170). Despite its great runoff efficiency, W260 has the lowest peak discharge, which may be attributable to delayed runoff or storage effects. W170 and W180 have greater peak flows (16.9 m³/s and 16.8 m³/s, respectively), indicating rapid runoff and flash flood concerns. W240 has the maximum efficiency but produces a low peak discharge of 2 m³/s, indicating a well-regulated hydrological response. At the outlet, the total runoff is 193.09 mm, with losses of 62.06 mm and a rainfall-runoff efficiency of 75.68%. The outlet's highest discharge is 65.9 m³/s, which includes flow contributions from upstream basins. This high number emphasizes the possibility of substantial downstream floods, contingent on flow regulation and storage capacity. The 2022-2023 modeling findings emphasize the geographical heterogeneity in hydrological behavior among basins. Basins like W240 and W260 use rainwater efficiently with little loss, whereas basins like W160 and W190 have more losses and lower efficiency. The outlet's high peak discharge emphasizes the significance of appropriate downstream flow management in reducing flood hazards and optimizing water resource availability.

3.4.3 Simulation run for the water year 2022- 2023

The simulation for 2022-2023 indicates variation in the hydrological responses of basins W160 to W270 and the outlet under 255.15 mm of uniform precipitation input, as represented in Table 7 and Fig. 5. Runoff values range from 166.62 mm in W160 to 229.05 mm in W240, and losses range from 26.1 mm in W240 to 88.53 mm in W160. Basins like W240 and W260 have the lowest losses and maximum runoff, indicating efficient water conversion systems. In contrast,

W160 and W190 exhibit larger losses, indicating significant infiltration or retention within their hydrological systems. Rainfall-runoff efficiency varies between 65.30% in W160 to 89.77% in W240. Basins W240 and W260 have exceptional efficiencies of 89.77% and 87.04%, showing a higher potential to convert rainfall into runoff. W160 has the lowest efficiency, at 65.30%, indicating higher losses and lesser runoff generation. Peak discharge levels range from 0.8 m^3/s (W260) to 16.9 m^3/s (W170).

Table 7 The result of a Simulation Run for the Year 2022-2023

Basin Name	Precipitation (mm)	Runoff (mm)	Loss (mm)	Rainfall/Runoff (%)	Peak Discharge (m^3/sec)
W160	255.15	166.62	88.53	65.30	12.2
W170	255.15	173.95	81.2	68.18	16.9
W180	255.15	181.81	73.34	71.26	16.8
W190	255.15	171.23	83.92	67.11	8.3
W200	255.15	173.89	81.26	68.15	5.9
W210	255.15	184.55	70.6	72.33	7.7
W220	255.15	179.57	75.58	70.38	5.3
W230	255.15	183.38	71.77	71.87	9.4
W240	255.15	229.05	26.1	89.77	2
W250	255.15	185.41	69.74	72.67	3.4
W260	255.15	222.09	33.06	87.04	0.8
W270	255.15	222.61	32.54	87.25	9
Outlet	255.15	193.09	62.06	75.68	65.9

Despite its great runoff efficiency, W260 has the lowest peak discharge, which may be attributable to delayed runoff or storage effects. W170 and W180 have greater peak flows (16.9 m^3/s and 16.8 m^3/s, respectively), indicating rapid runoff and flash flood concerns. W240 has the maximum efficiency but produces a low peak discharge of 2 m^3/s, indicating a well-regulated hydrological response. At the outlet, the total runoff is 193.09 mm, with losses of 62.06 mm and a rainfall-runoff efficiency of 75.68%. The outlet's highest discharge is 65.9 m^3/s, which includes flow contributions from upstream basins. This high number emphasizes the possibility of substantial downstream floods, contingent on flow regulation and storage capacity. The 2022-2023 modeling findings emphasize the geographical heterogeneity in hydrological behavior among basins. Basins like W240 and W260 use rainwater efficiently with little loss, whereas basins like W160 and W190 have more losses and lower efficiency. The outlet's high peak discharge emphasizes the significance of appropriate downstream flow management in reducing flood hazards and optimizing water resource availability.

In contrast, sub-basin W160's peak discharge remains steady at 25.6 m^3/s, indicating stable land cover and minor hydrological changes in the area. These findings highlight the growing impact of urbanization and impervious surface development on runoff dynamics, underlining the importance of sustainable urban design in mitigating possible flooding risks and managing increased surface runoff. Precipitation levels have a direct impact on runoff because rain is the principal source of surface runoff. Most watersheds experienced moderate runoff during 2017-2018, when precipitation totaled 260.46 mm. However, precipitation climbed to 619.56 mm between 2018 and 2019, resulting in a significant increase in runoff levels across all basins.

Fig. 5 impervious percent, runoff, and peak flow: a) impervious change chart, b) Runoff change chart, and c) Peak discharge change graph over years

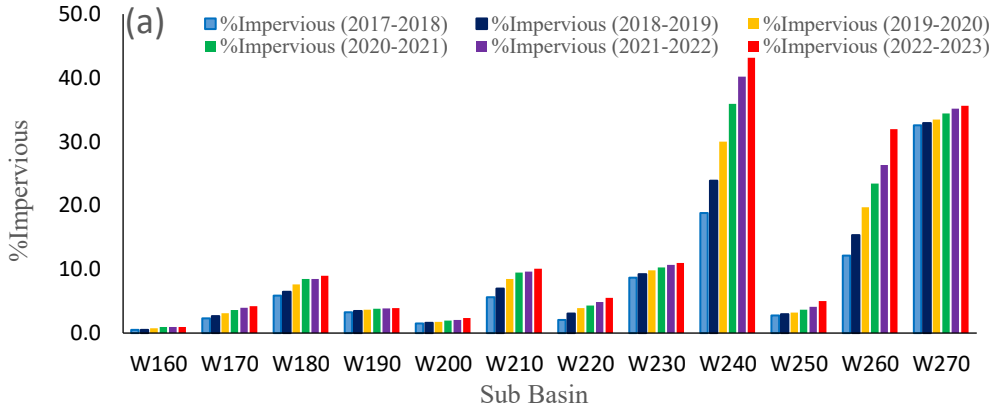

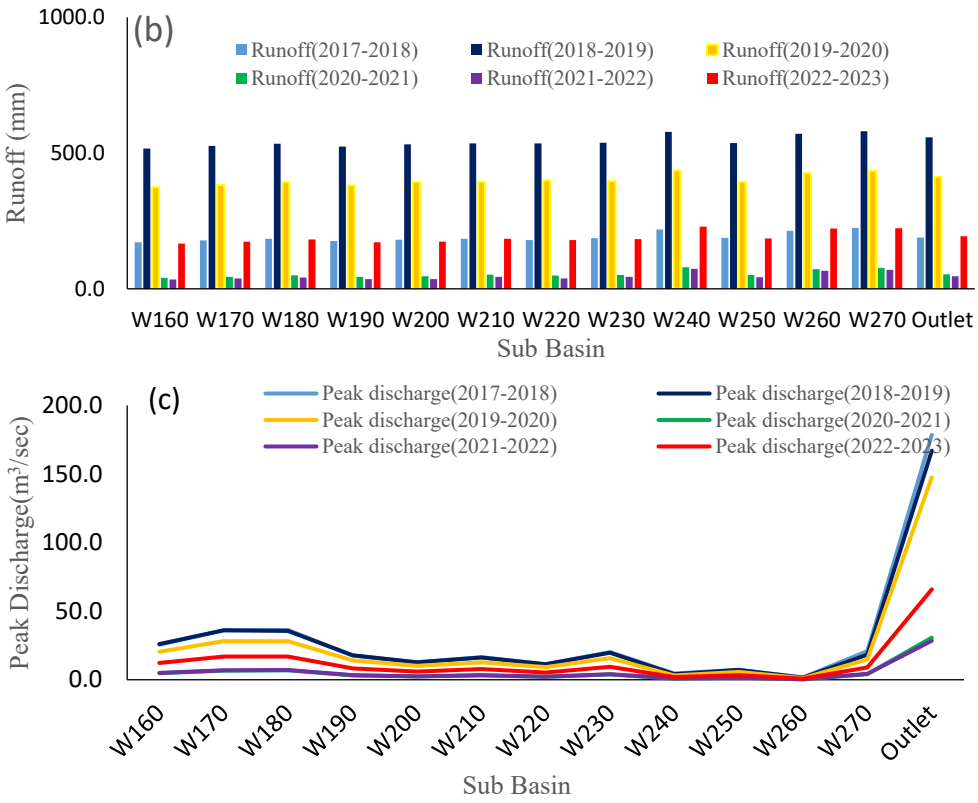

4. Conclusion

The main conclusions drawn from the HEC-HMS modeling on the Kalar urban basin are summarized as follows:

1. Between 2017 and 2023, urban areas increased from 25.87 to 39.81 km², crop land fluctuated from 154.25 to 45.21 km², barren land decreased from 29.26 to 10.14 km², and rangeland rose to 293.59 km², all contributing to significant hydrological changes.

2. The discrepancy between simulated and observed peak flow after model calibration was 9% with an R^2 of 0.9575. In addition, the peak flow difference between the simulated and observed values was 11% with the (R^2) of 0.9678 for the evaluated period.

3. Rainfall-runoff efficiency, measured by runoff percentages, increased from an average of 70% in 2017-2018 to higher levels in 2022-2023, particularly in basins with reduced losses like W270 (87.25%), W260 (87.04%), and W240 (from 83.68% to 89.77%). This change was driven by urban expansion, reduced barren land, and farmland shifts, leading to less infiltration, higher runoff efficiency, and altered hydrological responses.

4. The study shows that impervious surface expansion led to higher runoff, with peak discharge rising by 6.89% at the outlet and by 4.44% and 5.88% in sub-basins W240 and W260.

This study highlights the growing impact of urbanization and impervious surface development on runoff dynamics, underscoring the need for sustainable urban design to mitigate flood risks. However, it is limited by reliance on a single rainfall station near the outlet, which restricts capturing spatial rainfall variability and may affect modeling accuracy. Future research should establish additional rainfall stations to improve data accuracy, predict future land use and land cover (LULC) changes to assess their impact on surface runoff and flood risks, and develop serious water policy and planning strategies, particularly for sub-basins W240 and W60, to reduce flood probability and enhance runoff management.

Statements and Declarations

Data availability

Some or all data, models, or code that support the findings of this study are available from the corresponding author upon reasonable request.

Conflicts of interest

The author of this paper declared no conflict of interest regarding the authorship or publication of this paper.

Author contribution

S. M. Ali: Methodology, Data analysis, Writing - original draft; Mohsen Isari: Conceptualization, Methodology, Writing – review & editing; H. M. Rashid: Conceptualization, Methodology, Writing – review & editing; S. D. Parizadi: Writing – review & editing; J. Bharami: Conceptualization, Methodology, Writing – review & editing.

AI Use Declaration

During the preparation of this work, the author(s) used Grammarly to check and improve the grammar, style, and clarity of the manuscript. After using this tool, the author(s) reviewed and edited the content as needed and take(s) full responsibility for the content of the publication.

References

Alrammahi, F. S., & Hamdan, A. N. A. (2022, December). Simulation of rainfall-runoff in the Diyala River Basin in Iraq using hydrological model by HMS with remote sensing, Geo-HMS and ArcGIS. In *IOP Conference Series: Earth and Environmental Science, l*(1), p. 012007). IOP Publishing. https://doi.org/10.1088/1755-1315/1120/1/012007

Ahmadpari, H., & Khaustov, V. (2025). Agricultural Drought Monitoring Using Meteorological Indices in Darreh Dozdan Basin, Iran. *Advances in Civil Engineering and Environmental Science*, *2*(2), 72-84. https://doi.org/10.22034/acees.2025.512324.1022

Aswal, P., Saini, R., & Ansari, M. T. (2018). Spatio temporal monitoring of urban sprawl using GIS and remote sensing technique. *International Journal of Computer Applications*, *182*(27), 11-24. https://doi.org/10.5120/ijca2018918125

Aziz, S. F., Abdulrahman, K. Z., Ali, S. S., & Karakouzian, M. (2023). Water harvesting in the Garmian Region (Kurdistan, Iraq) using GIS and remote sensing. *Water*, *15*(3), 507. https://doi.org/10.3390/w15030507

Amini, A., & Hesami, A. (2017). The role of land use change on the sustainability of groundwater resources in the eastern plains of Kurdistan, Iran. *Environmental monitoring and assessment*, *189*(6), 297. https://doi.org/10.1007/s10661-017-6014-3

Amini, A., Ali, T. M., Ghazali, A. H. B., & Huat, B. K. (2009). Adjustment of peak streamflows of a tropical river for urbanization. American Journal of Environmental Sciences, 5(3), 285–294. https://doi.org/10.3844/ajessp.2009.285.294

Choudhari, K., Panigrahi, B., & Paul, J. C. (2014). Simulation of rainfall-runoff process using HEC-HMS model for Balijore Nala watershed, Odisha, India. *International Journal of Geomatics and Geosciences*, *5*(2), 253-265. http://ipublishing.co.in/jggsarticles/volfive/EIJGGS5021.pdf

Diriba, B. T. (2023). Assessment of rainfall-runoff process using Arc-GIS and HEC-HMS in Gelana Watershed, Rift Valley Basin, Ethiopia *Atmospheric and Oceanic Sciences. Bule Hora University.* https://doi.org/10.21203/rs.3.rs-3555518/v1

Haddad, A., & Remini, B. (2021). Extreme rainfall-runoff events modeling by HEC-HMS model for Koudiet Rosfa watershed, Algeria. *GeoScience Engineering*, *67*(4), 144-155. https://doi.org/10.35180/gse-2021-0060

Haitham, L., & Al-Mukhtar, M. (2022). Assessment of future climate change impacts on water resources of Khabour River catchment, north of Iraq. *Engineering and Technology Journal*, *40*(05), 695-709. https://doi.org/10.30684/etj.v40i5.1925

Hamdan, A. N. A., Almuktar, S., & Scholz, M. (2021). Rainfall-runoff modeling using the HEC-HMS model for the Al-Adhaim River catchment, northern Iraq. *Hydrology*, *8*(2), 58. https://doi.org/10.3390/hydrology copies8020058

Hu, S., & Shrestha, P. (2020). Examine the impact of land use and land cover changes on peak discharges of a watershed in the midwestern United States using the HEC-HMS model. *Papers in Applied Geography*, *6*(2), 101-118. https://doi.org/10.1080/23754931.2020.1732447

Ibrahim-Bathis, K., & Ahmed, S. A. (2016). Rainfall-runoff modelling of Doddahalla watershed—an application of HEC-HMS and SCN-CN in ungauged agricultural watershed. Arabian Journal of Geosciences, 9(3), 170. https://doi.org/10.1007/s12517-015-2228-2

Ibrahim-Bathis, K., & Ahmed, S. A. (2016). Rainfall-runoff modelling of Doddahalla watershed—an application of HEC-HMS and SCN-CN in ungauged agricultural watershed. *Arabian Journal of Geosciences*, *9*(3), 170. https://doi.org/10.1007/s12517-015-2228-2

Karami Moghadam, M., Amini, A., & Keshavarzi, A. (2020). Intake design attributes and submerged vanes effects on sedimentation and shear stress. *Water and Environment Journal*, *34*(3), 374-380. https://doi.org/10.1111/wej.12471

Khzr, B. O., Ibrahim, G. R. F., Hamid, A. A., & Ail, S. A. (2022). Runoff estimation using SCS-CN and GIS techniques in the Sulaymaniyah sub-basin of the Kurdistan region of Iraq. *Environment, Development and Sustainability*, *24*(2), 2640-2655. https://doi.org/10.1007/s10668-021-01549-z

Maher, M., Nasrallah, T. H., Rabah, M., & Abdelhaleem, F. S. (2022). Watershed delineation and runoff estimation of Wadi Tayyibah, South Sinai using Arc-GIS and HEC-HMS model. *Port-Said Engineering Research Journal*, *26*(2), 61-71. https://doi.org/10.21608/pserj.2022.111930.1155

Mohammed, F., Al-Manmi, D. A., Al-Manmi, A., & Hamasur, G. (2023). The Efficiency of SCS-CN, HEC-1, HEC-HMS, TR55, RATIONAL, and SNYDER UNIT Hydrograph Models for Determining Peak Flood Discharge in the Upper Part of Lesser Zab Basin, Kurdistan Region, Iraq. *Iraqi Bulletin of Geology and Mining*, *19*(1), 163-179. http://dx.doi.org/10.59150/ibgm1901a010

Mustafa, A., & Szydłowski, M. (2020). The impact of spatiotemporal changes in land development (1984–2019) on the increase in the runoff coefficient in Erbil, Kurdistan Region of Iraq. *Remote Sensing, 12(8)*, 1302. https://doi.org/10.3390/rs12081302

Mustafa, A., Szydłowski, M., Veysipanah, M., & Hameed, H. M. (2023). GIS-based hydrodynamic modeling for urban flood mitigation in fast-growing regions: a case study of Erbil, Kurdistan Region of Iraq. *Scientific reports*, *13*(1), 8935. https://doi.org/10.1038/s41598-023-36138-9

Odyuo, N. M. (2020). *Modelling the impact of land use land cover changes on th runoff processes of Chalakudy basin using HEC-HMS model* (Doctoral dissertation, Department of IDE).

http://14.139.181.140:8080//jspui/handle/123456789/1126

Ningaraju, H. J., & SB, G. K. (2016). Estimation of Runoff Using SCS-CN and GIS method in ungauged watershed: A case study of Kharadya mill watershed, India.

Patil, V. K., Saraf, V. R., Karad, O. V., Ghodke, S. B., Gore, D., & Dhekale, S. S. (2019). Simulation of rainfall runoff process using HEC-HMS model for Upper Godavari Basin Maharashtra, India. *European Journal of Engineering and Technology Research*, *4*(4), 102-107. https://doi.org/10.24018/ejeng.2019.4.4.927

Pal, B., & Samanta, S. (2011). Surface runoff estimation and mapping using remote sensing and geographic information system. *International Journal of Advances in Science and Technology*, *3*(2), 106-114.

Rashid, H. M. (2022). GIS Based Surface Runoff Estimation for Sulaimani City, KRG, Iraq. *Association of Arab Universities Journal of Engineering Sciences (JAARU)*, *29*(2). https://doi.org/10.33261/jaaru.2022.29.2.005

Ross, C. W., Prihodko, L., Anchang, J., Kumar, S., Ji, W., & Hanan, N. P. (2018). HYSOGs250m, global gridded hydrologic soil groups for curve-number-based runoff modeling. *Scientific data*, *5*(1), 1-9. https://doi.org/10.1038/sdata.2018.91

Gharibreza, M., Nasrollahi, A., Afshar, A., Amini, A., & Eisaei, H. (2018). Evolutionary trend of the Gorgan Bay (southeastern Caspian Sea) during and post the last Caspian Sea level rise. *Catena*, *166*, 339-348. https://doi.org/10.1016/j.catena.2018.04.016

Tassew, B. G., Belete, M. A., & Miegel, K. (2019). Application of HEC-HMS model for flow simulation in the Lake Tana basin: The case of Gilgel Abay catchment, upper Blue Nile basin, Ethiopia. *Hydrology, 6(1)*, 21. https://doi.org/10.3390/hydrology6010021

Cronshey, R. (1986). *Urban hydrology for small watersheds* (No. 55). US Department of Agriculture, Soil Conservation Service, Engineering Division. https://www.nrc.gov/docs/ML1421/ML14219A437.pdf

Wang, M., Zhang, L., & Baddoo, T. D. (2016). Hydrological modeling in a semi-arid region using HEC-HMS. *Journal of Water Resource and Hydraulic Engineering*, *5*(3), 105-115. https://doi.org/10.5963/JWRHE0503004